JOURNAL OF PROPULSION AND POWER
Vol. 16, No. 6, November–December 2000

Hub-Based Vibration Control of Multiple Rotating Airfoils

György Szász,* George T. Flowers,† and Roy J. Hartfield‡
Auburn University, Auburn, Alabama 36849

A study of vibration control of rotating airfoils using hub-based actuators (specifically, magnetic bearings) is presented. A simulation model consisting of a shaft/bladed disk assembly supported by two radial magnetic bearings and a thrust bearing is used to investigate the effectiveness and limitations of such an approach. Aerodynamic effects are accounted for with a simple model, and controllable vibration modes are determined. Deliberate patterned blade mistuning is identified as a possible strategy to increase system controllability/observability and to improve blade vibration suppression. A measure is developed to quantify relative controllability and observability to evaluate the potential effectiveness of the proposed mistuning strategy. Example simulation results are presented and discussed.

Nomenclature

A	=	state matrix
B	=	actuator control matrix
b	=	blade chord length
C	=	measurement matrix
$C(k)$	=	Theodorsen function
C_1	=	structural damping matrix
C_2	=	aerodynamic damping matrix
c, m	=	aerodynamic parameters
F_{X1}	=	horizontal force at radial bearing one
F_{X2}	=	horizontal force at radial bearing two
F_{Y1}	=	vertical force at radial bearing one
F_{Y2}	=	vertical force at radial bearing two
F_Z	=	axial force at thrust bearing
I_{Tbe}	=	tangential inertia of a blade with respect to its endpoint
I_{Th}	=	tangential inertia of hub
K_C	=	feedback gain for controller
K_O	=	feedback gain for observer
K_1	=	structural stiffness matrix
K_2	=	aerodynamic stiffness matrix
L_s	=	shaft length between radial bearings
l	=	blade length
M_1	=	structural mass matrix
M_2	=	aerodynamic mass matrix
m_b	=	mass of a blade
m_h	=	mass of hub
N	=	number of blades
n	=	rank of state matrix A
O	=	observability measure
P	=	controllability measure
p, q, r	=	multiblade coordinates
R	=	blade circle radius
$\boldsymbol{u}$	=	input vector
V	=	freestream air velocity
$\boldsymbol{v}$	=	row eigenvectors of state matrix A
$\boldsymbol{w}$	=	column eigenvectors of state matrix A
x, y, z	=	translational degrees of freedom of hub
$\boldsymbol{x}$	=	state vector
$\tilde{\boldsymbol{x}}$	=	state vector after multiblade transformation
$\boldsymbol{y}$	=	measurement vector
$\boldsymbol{z}$	=	estimated state vector
α, β	=	rotational degrees of freedom of hub about axes transverse to shaft
$\theta_{i,j}$	=	flap angle of jth blade of the ith set
ρ	=	fluid density
ψ	=	rotation angle of hub about main axis
Ω	=	spin speed
$\cdot$	=	time derivative

Presented as Paper 98-3312 at the AIAA/ASME/SAE/ASEE 34th Joint Propulsion Conference and Exhibit, Cleveland, OH, 13–15 July 1998; received 18 September 1998; revision received 25 November 1999; accepted for publication 20 December 1999.

*Graduate Research Assistant, Department of Mechanical Engineering, 201 Ross Hall.

†Associate Professor, Department of Mechanical Engineering, 201 Ross Hall.

‡Associate Professor, Aerospace Engineering Department, 211 Aerospace Engineering Building. Member AIAA.

Introduction

MORE than 40% of failures in gas turbines can be attributed to vibration-related blade failure, making it one of the major problems in turbomachinery.[1,2] Machine downtime and the replacement of damaged components associated with such failures can be extremely costly. In addition, for certain applications (such as jet engines) they can pose a severe safety risk. Blade vibration is also an important factor in engine noise, which is a major concern for aircraft applications. Clearly, an important area is the development of vibration suppression strategies for such systems. There is a large body of previous work in this area. The following overview is meant to provide a background for the current effort.

Vibration suppression for bladed-disk assemblies has traditionally been accomplished using such passive means as friction dampers attached to the blade. These techniques work reasonably well over a limited range of operation and a limited variation from design conditions, but result in generally suboptimal behavior for parametric configurations away from the nominal design.[3,4] Perhaps a more effective approach is the use of active means to provide vibration control. Magnetic bearings are a strong candidate for such applications.

There has been a great deal of recent activity in the application of magnetic bearings for the suppression of rotor vibration. Control strategies can be shaped to application specifics, providing flexible performance without changing bearing hardware. Humphris et al. conducted one of the earliest studies in the area, developing analog controllers to stabilize an active magnetic bearing (AMB)-supported rotor.[5] More recent works include that of Williams et al., who compared analog and digital controllers for vibration reduction in a radial AMB system.[6] In a recent paper, Flowers et al. give a comprehensive overview of the field of magnetic bearings with regard to rotor vibration control.[7]

The current research effort is concerned with the application of magnetic bearings to the vibration control of rotating airfoils. Of particular concern is developing a basic understanding of how such a strategy might be implemented and what problems must be overcome for it to be effective.

Basic Model

A conceptual model and a block diagram layout of the basic elements for bladed-disk vibration control with magnetic bearings is

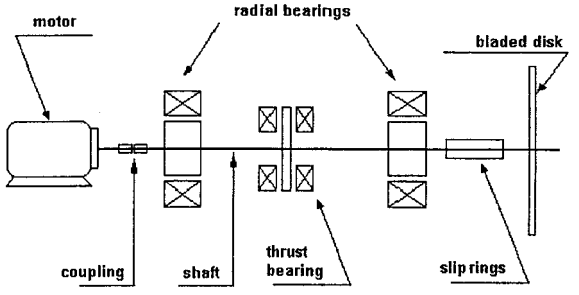

Fig. 1 Conceptual model for bladed-disk assembly.

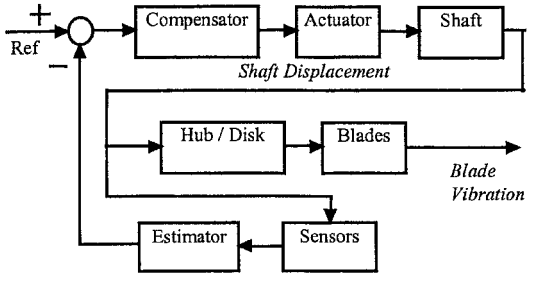

Fig. 2 Block diagram of basic components for bladed-disk vibration control.

shown in Figs. 1 and 2. They consist of 1) a controller or compensator, 2) the dynamics of the actuator (magnetic bearings), 3) the dynamics of the shaft, hub, disk, and blades, 4) sensors for measuring the shaft displacement, and 5) an observer for estimating the blade and hub states and the remaining unmeasured shaft states.

For this discussion, a basic model is developed in the following sections. It consists of a rigid disk with rigid blades distributed symmetrically around the rim of the disk. The blades are attached to the disk with pin connections and held in place with springs attached to the root of each blade. For the following model development, only the flapping modes are considered. These modes are assumed to be uncoupled from each other, that is, there is no interblade coupling. Aerodynamic effects are also included.

Structural Model

The resulting equations of motion, formulated in a Lagrangian fashion, take on the following matrix form:

$$M_1\ddot{\boldsymbol{x}} + C_1\dot{\boldsymbol{x}} + K_1\boldsymbol{x} = B_1\boldsymbol{u} \tag{1}$$

where

$$\boldsymbol{x} = [x \quad y \quad z \quad \alpha \quad \beta \quad \theta_1 \quad \cdots \quad \theta_N]^T$$

and

$$\boldsymbol{u} = [F_{X1} \quad F_{Y1} \quad F_{X2} \quad F_{Y2} \quad F_Z]^T$$

Expanded expressions for M, C, and K are

$$M_1 = \left[\begin{array}{ccc:cc:ccc} m_h + Nm_b & 0 & 0 & 0 & 0 & 0 & \cdots & 0 \\ 0 & m_h + Nm_b & 0 & 0 & 0 & 0 & \cdots & 0 \\ 0 & 0 & m_h + Nm_b & 0 & 0 & -\frac{1}{2}m_b l & \cdots & -\frac{1}{2}m_b l \\ \hdashline 0 & 0 & 0 & I_{\mathrm{Th}} + (N/2)I_{\mathrm{Tbe}} & 0 & I_{\mathrm{Tbe}}\cos\psi_1 & \cdots & I_{\mathrm{Tbe}}\cos\psi_N \\ 0 & 0 & 0 & 0 & I_{\mathrm{Th}} + (N/2)I_{\mathrm{Tbe}} & -I_{\mathrm{Tbe}}\sin\psi_1 & \cdots & -I_{\mathrm{Tbe}}\sin\psi_N \\ \hdashline 0 & 0 & -\frac{1}{2}m_b l & I_{\mathrm{Tbe}}\cos\psi_1 & I_{\mathrm{Tbe}}\sin\psi_1 & I_{\mathrm{Tbe}} & 0 & 0 \\ \vdots & \vdots & \vdots & \vdots & \vdots & 0 & \ddots & 0 \\ 0 & 0 & -\frac{1}{2}m_b l & I_{\mathrm{Tbe}}\cos\psi_N & I_{\mathrm{Tbe}}\sin\psi_N & 0 & 0 & I_{\mathrm{Tbe}} \end{array}\right]$$

$$C_1 = \left[\begin{array}{ccc:cc:ccc} 0 & 0 & 0 & 0 & 0 & 0 & \cdots & 0 \\ 0 & 0 & 0 & 0 & 0 & 0 & \cdots & 0 \\ 0 & 0 & 0 & 0 & 0 & 0 & \cdots & 0 \\ \hdashline 0 & 0 & 0 & 0 & (-NI_{\mathrm{Tbe}} + I_{Ph})\Omega & 0 & \cdots & 0 \\ 0 & 0 & 0 & (NI_{\mathrm{Tbe}} + I_{Ph})\Omega & 0 & 0 & \cdots & 0 \\ \hdashline 0 & 0 & 0 & -I_{\mathrm{Tbe}}\Omega\sin\psi_1 & -I_{\mathrm{Tbe}}\Omega\cos\psi_1 & 0 & 0 & 0 \\ \vdots & \vdots & \vdots & \vdots & \vdots & 0 & \ddots & 0 \\ 0 & 0 & 0 & -I_{\mathrm{Tbe}}\Omega\sin\psi_N & -I_{\mathrm{Tbe}}\Omega\cos\psi_N & 0 & 0 & 0 \end{array}\right]$$

$$K_1 = \left[\begin{array}{ccc:cc:ccc} 0 & 0 & 0 & 0 & 0 & 0 & \cdots & 0 \\ 0 & 0 & 0 & 0 & 0 & 0 & \cdots & 0 \\ 0 & 0 & 0 & 0 & 0 & 0 & \cdots & 0 \\ \hdashline 0 & 0 & 0 & 0 & 0 & I_{\mathrm{Tbe}}\cos\psi_1\Omega^2 & \cdots & I_{\mathrm{Tbe}}\cos\psi_N\Omega^2 \\ 0 & 0 & 0 & 0 & 0 & -I_{\mathrm{Tbe}}\sin\psi_1\Omega^2 & \cdots & -I_{\mathrm{Tbe}}\sin\psi_N\Omega^2 \\ \hdashline 0 & 0 & 0 & 0 & 0 & K_i + I_{\mathrm{Tbe}}\Omega^2 & 0 & 0 \\ \vdots & \vdots & \vdots & \vdots & \vdots & 0 & \ddots & 0 \\ 0 & 0 & 0 & 0 & 0 & 0 & 0 & K_i + I_{\mathrm{Tbe}}\Omega^2 \end{array}\right]$$

The structural model is a rigid model of the hub coupled by varying stiffness flexures to rigid models of the blades. Matrix B_1 assumes a system configuration similar to Fig. 1.

$$B_1 = \begin{bmatrix} 1 & 0 & 1 & 0 & 0 \\ 0 & 1 & 0 & 1 & 0 \\ 0 & 0 & 0 & 0 & 1 \\ L_s/2 & 0 & -L_s/2 & 0 & 0 \\ 0 & L_s/2 & 0 & -L_s/2 & 0 \\ 0 & 0 & 0 & 0 & 0 \\ \vdots & \vdots & \vdots & \vdots & \vdots \\ 0 & 0 & 0 & 0 & 0 \end{bmatrix}$$

The horizontal and vertical forces are obtained by formulating the sums

$$\sum_i F_{Xi}, \qquad \sum_i F_{Yi}$$

respectively, whereas the axial force is simply F_Z. Moments are generated by multiplying the forces with their respective arms.

Aerodynamic Model

A comprehensive discussion of advanced concepts for the treatment of aeroelasticity in turbomachines is given by Carta[8]; however,

a simplified version of a portion of the classical Theodorsen theory for aeroelasticity has been selected as the most practical approach for demonstrating the basic idea of controlling aerodynamically induced vibrations.[9]

The basic conceptual argument of the Theodorsen method is that a coalescence of the torsion branch frequencies with the bending branch frequencies will result in a flutter point and substantial aerodynamically induced vibrations. In principle then, control of either torsion or bending could result in the controllability of aerodynamically induced vibrations. The hub-based control strategy presented herein does not address the controllability of the torsion branch oscillations; however, active input forces aimed at controlling the bending mode are possible (as discussed earlier). Hence, the proposed strategy is to control the bending mode to prevent excessive vibrations.

From the Theodorsen model, the bending mode aerodynamic forcing term is modeled as

$$F_a = c\dot{h} + m\ddot{h}$$

where

$$m = -\pi\rho b^3, \qquad c = -2\pi\rho b^2 V C(k)$$

and h is a reference point on a blade. The Theodorsen function $C(k)$ is complex, and the retention of this function allows for the inclusion of aerodynamic stiffness; however, to a first approximation, the complex function may be approximated as unity and any aerodynamic stiffness terms will arise solely from mathematical manipulations necessary for control purposes. Because controllability is the primary issue at hand, the Theodorsen function is taken to be unity, and the model as described has been implemented.

Forming the virtual work expression yields a set of generalized forces that can be decomposed into linear augmentations of the existing system matrices. The resulting mass, stiffness, and damping matrices are

$$K_2 = \begin{bmatrix}
0 & 0 & 0 & 0 & 0 & 0 & \cdots & 0 \\
0 & 0 & 0 & 0 & 0 & 0 & \cdots & 0 \\
0 & 0 & 0 & 0 & 0 & -\tfrac{1}{2}R^2 m\omega^2 & \cdots & -\tfrac{1}{2}R^2 m\omega^2 \\
\hdashline
0 & 0 & 0 & 0 & 0 & \tfrac{1}{3}R^3 m\omega^2 \cos\psi_1 & \cdots & \tfrac{1}{3}R^3 m\omega^2 \cos\psi_N \\
0 & 0 & 0 & 0 & 0 & -\tfrac{1}{3}R^3 m\omega^2 \sin\psi_1 & \cdots & -\tfrac{1}{3}R^3 m\omega^2 \sin\psi_N \\
\hdashline
0 & 0 & 0 & 0 & 0 & \tfrac{1}{3}R^3 m\omega^2 & 0 & 0 \\
\vdots & \vdots & \vdots & \vdots & \vdots & 0 & \ddots & 0 \\
0 & 0 & 0 & 0 & 0 & 0 & 0 & \tfrac{1}{3}R^3 m\omega^2
\end{bmatrix}$$

Incorporation of the aerodynamic terms into the equations of motions yields

$$[M_1 - M_2]\ddot{\boldsymbol{x}} + [C_1 - C_2]\dot{\boldsymbol{x}} + [K_1 - K_2]\boldsymbol{x} = B_1\boldsymbol{u} \qquad (2)$$

as the linearized equations of motion for the complete model.

Examination and numerical simulation of these equations reveals two potential problems. First, not all of the vibration modes are controllable and observable from hub-based actuation and sensing. Second, the matrices are time varying, which denies the possibility of applying traditional control techniques. Each of these issues are addressed, in turn, with the following discussion.

Controllability and Observability

To suppress bladed-disk vibration using hub-based actuation, the actuator must have sufficient bandwidth to pass the control signal to the plant (shaft, hub/disk, and blades). This issue is discussed in some detail by Szász and Flowers.[10] The dynamics of the shaft

$$M_2 = \begin{bmatrix}
0 & 0 & 0 & 0 & 0 & 0 & \cdots & 0 \\
0 & 0 & 0 & 0 & 0 & 0 & \cdots & 0 \\
0 & 0 & NRm & 0 & 0 & -\tfrac{1}{2}R^2 m & \cdots & -\tfrac{1}{2}R^2 m \\
\hdashline
0 & 0 & 0 & (N/6)R^3 mc & 0 & \tfrac{1}{3}R^3 m\cos\psi_1 & \cdots & \tfrac{1}{3}R^3 m\cos\psi_N \\
0 & 0 & 0 & 0 & (N/6)R^3 m & -\tfrac{1}{3}R^3 m\sin\psi_1 & \cdots & -\tfrac{1}{3}R^3 m\sin\psi_N \\
\hdashline
0 & 0 & -\tfrac{1}{2}R^2 m & \tfrac{1}{3}R^3 m\cos\psi_1 & -\tfrac{1}{3}R^3 m\sin\psi_1 & (R^3/3)m & 0 & 0 \\
\vdots & \vdots & \vdots & \vdots & \vdots & 0 & \ddots & 0 \\
0 & 0 & -\tfrac{1}{2}R^2 m & \tfrac{1}{3}R^3 m\cos\psi_N & -\tfrac{1}{3}R^3 m\sin\psi_N & 0 & 0 & (R^3/3)m
\end{bmatrix}$$

$$C_2 = \begin{bmatrix}
0 & 0 & 0 & 0 & 0 & 0 & \cdots & 0 \\
0 & 0 & 0 & 0 & 0 & 0 & \cdots & 0 \\
0 & 0 & -NRc & 0 & 0 & -(R^2/2)c & \cdots & -(R^2/2)c \\
\hdashline
0 & 0 & 0 & (N/6)R^3 c & (N/3)R^3 m\omega^2 & \tfrac{1}{3}R^3 c\cos\psi_1 & \cdots & \tfrac{1}{3}R^3 c\cos\psi_N \\
0 & 0 & 0 & -(N/3)R^3 m\omega^2 & (N/6)R^3 c & -\tfrac{1}{3}R^3 c\sin\psi_1 & \cdots & -\tfrac{1}{3}R^3 c\sin\psi_N \\
\hdashline
0 & 0 & -\tfrac{1}{2}R^2 c & \tfrac{1}{3}R^3 c\cos\psi_1 \\ -\tfrac{2}{3}R^3 m\omega\sin\psi_1 & -\tfrac{1}{3}R^3 c\sin\psi_1 \\ -\tfrac{2}{3}R^3 m\omega\cos\psi_1 & & \tfrac{1}{3}R^3 c & 0 & 0 \\
\vdots & \vdots & \vdots & \vdots & \vdots & 0 & \ddots & 0 \\
0 & 0 & -\tfrac{1}{2}R^2 c & \tfrac{1}{3}R^3 c\cos\psi_N \\ -\tfrac{2}{3}R^3 m\omega\sin\psi_N & -\tfrac{1}{3}R^3 c\sin\psi_N \\ -\tfrac{2}{3}R^3 m\omega\cos\psi_N & & 0 & 0 & \tfrac{1}{3}R^3 c
\end{bmatrix}$$

and hub also play a significant role in the effectiveness of any blade vibration control strategy. These components serve to filter high-frequency control forces from the bladed disk and any high-frequency bladed-disk vibration from measurement and estimation using shaft-based sensors. Consequently, it is inherently a very difficult problem to estimate and control bladed-disk vibration modes at frequencies above the combined actuator/shaft/hub fundamental frequency.

A possible strategy is to consider only bladed disk vibration modes that are below the combined shaft/hub fundamental frequency. However, even for such cases, multiple-bladed disk assemblies (with identical blades) are subject to a variety of vibration modes, many of which are not reachable by any type of hub-based actuation. Simulation testing has shown that a bladed disk with more than three identical blades has fundamental blade vibration modes that uncouple from the hub. Figures 3 and 4 show bladed-disk vibration modes that couple with the hub and are controllable and observable using magnetic bearings and shaft-based sensors. The mode shown in Fig. 3 could be controlled with an axially applied force (thrust bearing) and sensed using an axial shaft position measurement. The mode shown in Fig. 4 can be controlled using a moment applied to the shaft (via radial magnetic bearings) and sensed with several measurements of the shaft radial position. On the other hand, Fig. 5 shows a vibration mode that is not controllable and observable from shaft-based actuation and sensing. The

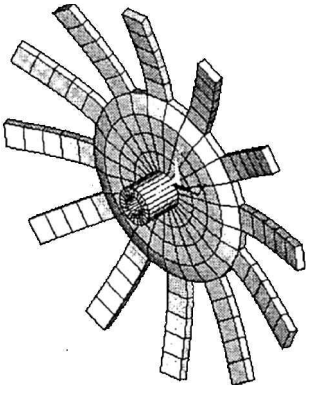

Fig. 3 First controllable flap mode.

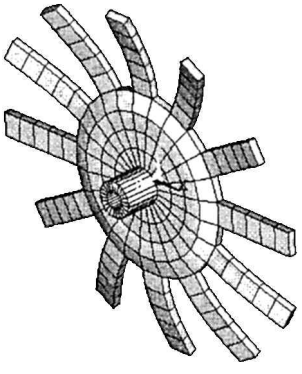

Fig. 4 Second controllable flap mode.

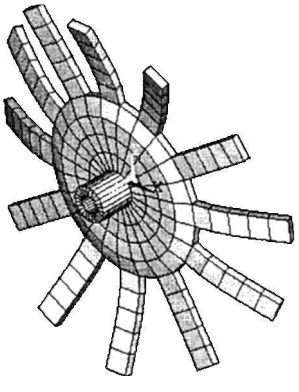

Fig. 5 Uncontrollable flap mode.

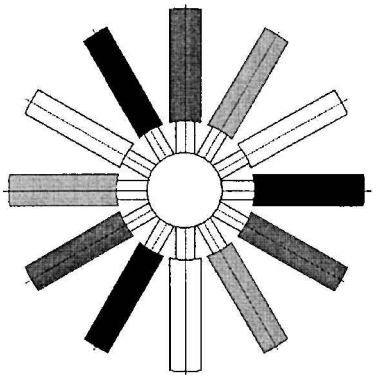

Fig. 6 Mistuning pattern for full controllability.

inertial forces exerted by the blades cancel each other and impart no dynamic loading to the shaft.

A basic issue is how one might enhance coupling between the shaft and blade vibrations. Pierre and Murthy discuss the vibration localization that may occur in mistuned bladed-disk assemblies.[11] Deliberate mistuning has been suggested as a possible means of alleviating some vibration problems. Such ideas lend themselves readily as possible solutions to the controllability problem. The introduction of mistuning into a bladed-disk assembly (by having slightly dissimilar blade stiffness values, for example), depending on the extent of the dissimilarity of the blades, may even produce full controllability of the system.[10] It is proposed that a deliberate and pattern mistuning be used to enhance the controllability and observability of bladed-disk vibration from shaft-based actuation and sensing. For reasons that will be discussed later, the blades should be divided into groups of three identically mistuned blades at locations symmetrically spaced (120 deg apart) around the circumference of the disk. The suggested pattern is shown in Fig. 6. Blades of similar shade have the same properties.

Involuntary (or random) mistuning is a significant problem with bladed-disk assemblies. For most bladed-disk systems, the level of involuntary mistuning is less than 1–2%. Mistuning may significantly alter the forced response characteristics of bladed-disk systems and, depending on the mistuning pattern, may increase or decrease maximum response levels.[12] An important question is the effectiveness of deliberate mistuning in the presence of such involuntary mistuning. From the perspective of this discussion, the worst pattern for involuntary mistuning is one that brings the blade sets closer to a tuned configuration.

To assess the effectiveness of the suggested mistuning pattern, a measure of relative controllability and observability applicable to the current situation must be established. The Popov-Belevitch-Hautus (PBH) eigenvector test, described by Kalaith,[13] for full controllability requires that each row (or left) eigenvector of the system state matrix A not be orthogonal to the control matrix B. Likewise, the test for full observability requires that each column (or right) eigenvector of the system state matrix not be orthogonal to the measurement matrix C.

A relative controllability measure based on this test was described by Szász and Flowers.[10] The approach is modified and extended here to describe both relative controllability and relative observability in a rigorous fashion.

For this purpose, we examine the dot product of the eigenvectors of the model A matrix with the model B matrix. The maximum absolute value of the dot product of each row eigenvector with the B matrix is taken as the relative controllability of that mode. The values obtained for all of the system eigenvectors are compared, and the minimum value is taken to be the relative controllability of the entire system with regard to the specified actuator configuration. Accordingly, we define a relative controllability measure P as

$$P = \min\{\max[\text{abs}(v_i B)]\}_{i=1,\ldots,n}$$

where v_i is a row eigenvector of A as its columns and n is the rank of A.

A similar quantity can be defined for the relative observability as

$$O = \min\{\max[\text{abs}(w_i' C)]\}_{i=1,1,\ldots,n}$$

where w_i is a column eigenvector of A as its columns and n is the rank of A.

These controllability and observability measures were applied to the basic model that was developed in the preceding sections. The following observations were made.

1) Increasing the mistuning level (according to the proposed mistuning pattern) generally serves to enhance controllability and observability.

2) The controllability and observability measures tend to asymptotically approach an upper limit, and increasing mistuning beyond a certain level does little to enhance these measures.

The next question that naturally arises is the general applicability of these results. That is, are similar characteristics observed for more complex models, particularly for cases where multiple blade vibration modes are important. To address this concern, the preceding controllability and observability measures are applied to the model shown in Fig. 7. It consists of a rigid disk with spring–mass systems (representing the blades) located at regular intervals around the disk. The multiple spring–mass arrangement allows for the consideration of multiple blade modes.

Through the use of this model, some results for various mistuning levels are shown in Figs. 8 and 9. For this example, each blade has a mass of 20 g. Each root spring has a nominal stiffness of 6.3 N/m, and all other blade springs have a stiffness of 12.6 N/m. The hub has a mass of 2.5 kg and a transverse moment of inertia of 0.1 kg-m^2. The disk has 12 blades, and each blade has 5 mass stations. The mistuning level represents the maximum percentage above or below the nominal stiffness value for any of the blade sets. For example, a mistuning level of 5% (for four 3-bladed assemblies) means that stiffness values of 0.95, 0.975, 1.025, and 1.05 were used.

The controllability and observability measures shown in Figs. 8 and 9 are normalized by the P and O values, respectively, at a mistuning level of 5%. The results are similar to those described earlier for the basic model, but there are some differences. In Fig. 8, as the mistuning level increases, the controllability measure increases steadily until the mistuning level is about 5%. At this point, it reaches a peak and begins to decrease slowly, a result not observed for the basic model. This appears to be due to the filtering effect that results from the softer root springs (as compared to the other blade springs). As the mistuning level increases, the stiffnesses associated with two of the root springs decrease, and the forces transmitted from the hub have less effect on the higher frequency dynamics associated with the upper blade stations. The increased modal separation provided by the mistuning is overcome by this effect, and the overall system controllability begins to decrease. Similar results for the observability measure are seen in Fig. 9. Beyond a certain level of mistuning, less of the higher frequency blade dynamics can be transmitted to the hub through the blade roots, resulting in reduced observability for those modes. However, the decrease in controllability/observability that results from such effects tends to be minor, and the observations described earlier for the basic model hold up quite well even for this substantially more complex dynamic system.

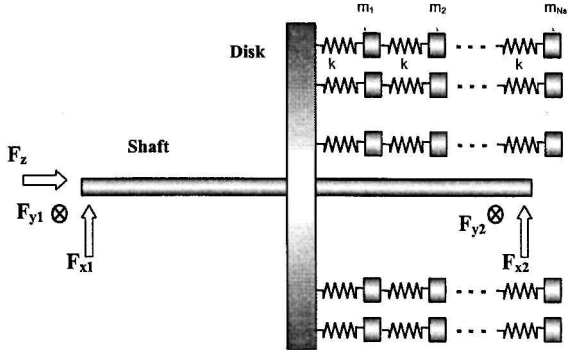

Fig. 7 Blade-disk model with multiple spring–mass blades.

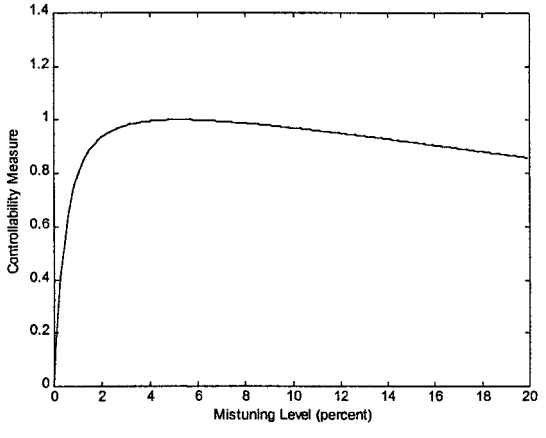

Fig. 8 Mistuning level and relative controllability.

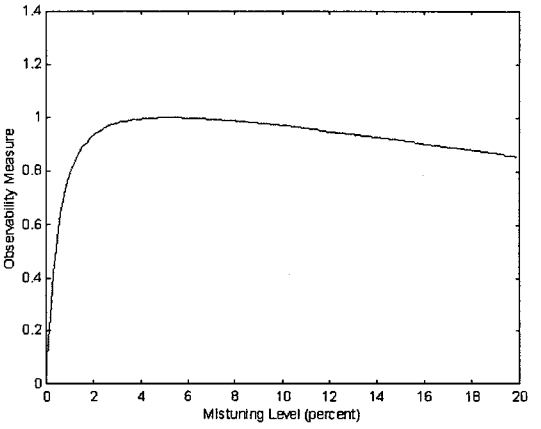

Fig. 9 Mistuning level and relative observability.

Note that the relative controllability and observability of the blade states is quite small for reasonable levels of mistuning. However, the major point is that, without mistuning, some of the blade states are completely uncontrollable and observable. The introduction of the proposed mistuning pattern introduces structural controllability/observability in a form that can potentially produce appreciable blade vibration suppression.

Transformed Equations

The second issue of concern is the time periodic nature of the described model. To use traditional constant coefficient control techniques, the equations themselves have to be in constant coefficient form. In the present case, this can be achieved through the multiblade transform.[14] The multiblade transformation replaces the displacement states associated with individual blades with states associated with blade system vibration modes. One may also view the transformation as replacing the dynamic variables referenced to a rotating frame with those referenced to a space-fixed frame.

The maximum number of identical blades that can be controlled using hub-based actuators is three, and the minimum number of blades that allow the use of the multiblade transformation is also three. Dividing the blades into controllable groups of three (by varying the root stiffness values associated with each set) therefore suggests itself as a solution to both the controllability and the transformability problem. This is, of course, provided that the disk has a number of blades that is an integer multiple of three.

The multiblade coordinates applicable to the multiple three-bladed systems described are

$$p_i = \sum_{j=1}^{N} \theta_{i,j}, \qquad q_i = \sum_{j=1}^{N} \theta_{i,j} \cos \psi_{i,j}, \qquad r_i = \sum_{j=1}^{N} \theta_{i,j} \sin \psi_{i,j}$$

where the index i indicates a particular three-bladed set. Applying this transformation to Eq. (1) gives

$$M_1' = \begin{bmatrix}
m_T & & & & & & & & & \\
& m_T & & & & & & & & \\
& & m_T & & & -\tfrac{1}{2}ml & \cdots & -\tfrac{1}{2}ml & & \\
& & & I_T & & & & & I_B \cdots I_B & \\
& & & & I_T & & & & & -I_B \cdots -I_B \\
-(N/2)ml & & & & & I_B & & & & \\
\vdots & & & & & & \ddots & & & \\
-(N/2)ml & & & & & & & I_B & & \\
& & & (N/2)I_B & & & & & I_B & \\
& & & \vdots & & & & & \ddots & \\
& & & (N/2)I_B & & & & & & I_B \\
& & & & -(N/2)I_B & & & & & I_B \\
& & & & \vdots & & & & & \ddots \\
& & & & -(N/2)I_B & & & & & & I_B
\end{bmatrix}$$

$$C_1' = \begin{bmatrix}
 & & & & & & & \\
 & -(NI_{\mathrm{Tbe}} + I_{Ph})\Omega & & & & & 2I_B\Omega \cdots 2I_B\Omega \\
 & (NI_{\mathrm{Tbe}} + I_{Ph})\Omega & & & 2I_B\Omega \cdots 2I_B\Omega & & \\
 & & & & & & \\
 & -(N/2)I_B\Omega & & & & & 2I_B\Omega \\
 & \vdots & & & & & \ddots \\
 & -(N/2)I_B\Omega & & & & & 2I_B\Omega \\
 & -(N/2)I_B\Omega & & & -2I_B\Omega & & \\
 & \vdots & & & \ddots & & \\
 & -(N/2)I_B\Omega & & & -2I_B\Omega & &
\end{bmatrix}$$

$$K_1' = \begin{bmatrix}
 & & & & & \\
 & & & & & \\
 & & K_1 + I_B\Omega^2 & & & \\
 & & \ddots & & & \\
 & & K_n + I_B\Omega^2 & & & \\
 & & & K_1 & & \\
 & & & \ddots & & \\
 & & & K_n & & \\
 & & & & K_1 & \\
 & & & & \ddots & \\
 & & & & K_n &
\end{bmatrix}$$

with the new state vector

$$\tilde{\boldsymbol{x}}[x \quad y \quad z \quad \alpha \quad \beta \quad p_1, \ldots, p_N \quad q_1, \ldots, q_N \quad r_1, \ldots, r_N]^T$$

The matrices containing the aerodynamic forcing terms are also transformed to get

$$M_2' = \begin{bmatrix} NRm & & -\frac{1}{2}R^2m \cdots -\frac{1}{2}R^2m & & \\ & (N/6)R^3m & & \frac{1}{3}R^3m \cdots \frac{1}{3}R^3m & \\ & \qquad (N/6)R^3m & & & -\frac{1}{3}R^3m \cdots -\frac{1}{3}R^3m \\ -(N/2)R^2m & & \frac{1}{3}R^3m & & \\ \vdots & & \ddots & & \\ -(N/2)R^2m & & \qquad \frac{1}{3}R^3m & & \\ & (N/6)R^3m & & \frac{1}{3}R^3m & \\ & \vdots & & \ddots & \\ & (N/6)R^3m & & \qquad \frac{1}{3}R^3m & \\ & -(N/6)R^3m & & & \frac{1}{3}R^3m \\ & \vdots & & & \ddots \\ & -(N/6)R^3m & & & \qquad \frac{1}{3}R^3m \end{bmatrix}$$

$$C_2' = \begin{bmatrix} -NRc & & -\frac{1}{2}R^2c \cdots -\frac{1}{2}R^2c & & \\ & (N/6)R^3m \quad (N/6)R^3m\omega & & \frac{1}{3}R^3c \cdots \frac{1}{3}R^3c & \frac{2}{3}R^3m\omega \cdots \frac{2}{3}R^3m\omega \\ & -\frac{N}{3}R^3m\omega \quad -\frac{N}{6}R^3m & & \frac{2}{3}R^3m\omega \cdots \frac{2}{3}R^3m\omega & -\frac{1}{3}R^3c \cdots -\frac{1}{3}R^3c \\ -(N/2)R^2c & & \frac{1}{3}R^3c & & \\ \vdots & & \ddots & & \\ -(N/2)R^2c & & \qquad \frac{1}{3}R^3c & & \\ & (N/6)R^3c \quad -(N/3)R^3m\omega & & \frac{1}{3}R^3c & \frac{2}{3}R^3m\omega \\ & \vdots \qquad \vdots & & \ddots & \ddots \\ & (N/6)R^3c \quad -(N/3)R^3m\omega & & \qquad \frac{1}{3}R^3c & \qquad \frac{2}{3}R^3m\omega \\ & -(N/3)R^3m\omega \quad -(N/6)R^3c & & -\frac{2}{3}R^3m\omega & \frac{1}{3}R^3c \\ & \vdots \qquad \vdots & & \ddots & \ddots \\ & -(N/3)R^3m\omega \quad (N/6)R^3c & & \qquad -\frac{2}{3}R^3m\omega & \qquad -\frac{1}{3}R^3c \end{bmatrix}$$

$$K_2' = \begin{bmatrix} & & -\frac{1}{2}R^2m\omega^2 \cdots -\frac{1}{2}R^2m\omega^2 & & \\ & & & & \frac{1}{3}R^3c\omega \cdots \frac{1}{3}R^3c\omega \\ & & & \frac{1}{3}R^3c\omega \cdots \frac{1}{3}R^3c\omega & \\ & & \frac{1}{3}R^3m\omega & & \\ & & \ddots & & \\ & & \qquad \frac{1}{3}R^3m\omega & & \\ & & & & \frac{1}{3}R^3c\omega \\ & & & & \ddots \\ & & & & \qquad \frac{1}{3}R^3c\omega \\ & & & -\frac{1}{3}R^3m\omega^2 & \\ & & & \ddots & \\ & & & \qquad -\frac{1}{3}R^3m\omega^2 & \end{bmatrix}$$

The resulting equations of motion are

$$[M_1 - M_2]\ddot{\tilde{x}} + [C_1 - C_2]\dot{\tilde{x}} + [K_1 - K_2]\tilde{x} = B_1 u \qquad (3)$$

These matrices are now constant coefficient, and traditional linear analysis and control techniques can be applied.

Analysis and Simulation Results

To illustrate the effectiveness of the strategy described and demonstrate the implementation procedure, some results from simulation studies are presented. State-space controller design methods, which will be used for this discussion, are based on a first-order representation of the equations of motion. Conversion of the given mathematical model yields the new form

$$\dot{\tilde{x}} = A\tilde{x} + Bu, \qquad y = C\tilde{x}, \qquad u = -K_C z$$

$$\dot{z} = Az - CK_O(z - \tilde{x}) + Bu \qquad (4)$$

where

$$A = \left[\begin{array}{c:c} 0 & I_{N+5} \\ \hdashline -(M_1' - M_2')^{-1}(K_1' - K_2') & -(M_1' - M_2')^{-1}(C_1' - C_2') \end{array}\right]$$

$$B = \left[\begin{array}{c} 0 \\ \hdashline (M_1' - M_2')^{-1} B_1 \end{array}\right], \qquad C = [I_{5,N+5} \vdots 0]$$

The states are estimated using a full-state observer with a feedback gain of K_O. To demonstrate this methodology, the response to an initial disturbance of a 12-bladed disk spinning at 1000 rpm was simulated. The stabilizing control gains K_C were determined using pole placement. Note that the actuators that provide the control forces also serve to support the rotor. As a result, any control strategy must include two basic components. The first stabilizes the rotor and provides acceptable rotordynamic characteristics. The second serves to provide the blade vibration suppression. Example responses are shown in Figs. 10 and 11. For clarity, only example hub and blade states are shown. The behavior of the other hub and blade states is similar to the example states. A mistuning level of 10% was used. The disk has a mass of 2.5 kg, a transverse moment of inertia of 0.1, and a polar moment of inertia of 0.15. The blades each have a mass of 20 g and a nominal root stiffness of 6.3 N/m.

As discussed in the preceding sections, the proposed mistuning pattern enhances the controllability and observability of the blade vibrations using hub-based actuation and sensing. As a result, any motions of the blades will cause some motion of the hub. One might suppose that, if the hub vibration is suppressed, so will be the blade vibration. However, the effectiveness of such a strategy is extremely limited due to the relatively small effect that some of the blade modes will have on the hub motion. Figure 10 shows a blade vibration mode of the system with only the first component of the control system active, that is, no feedback of the blade states into the controller. A typical response of a blade to an initial displacement is shown. As shown in Fig. 10a, the hub states tend to converge quite swiftly to a small and almost steady (very slow decay rate) oscillation induced by the coupling between the blade and hub states. The states

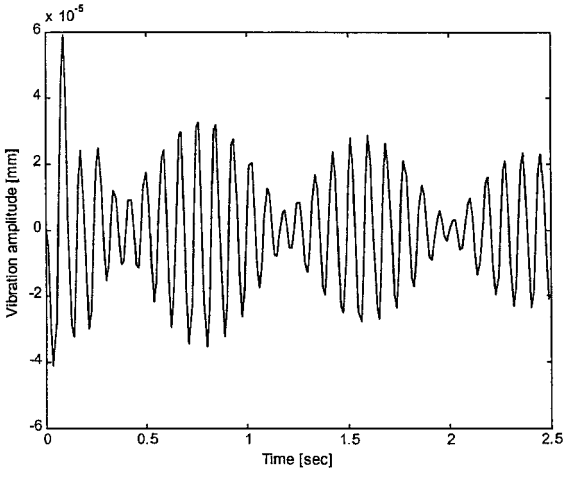

Fig. 10a Hub vibration without blade state feedback; hub axial displacement is shown.

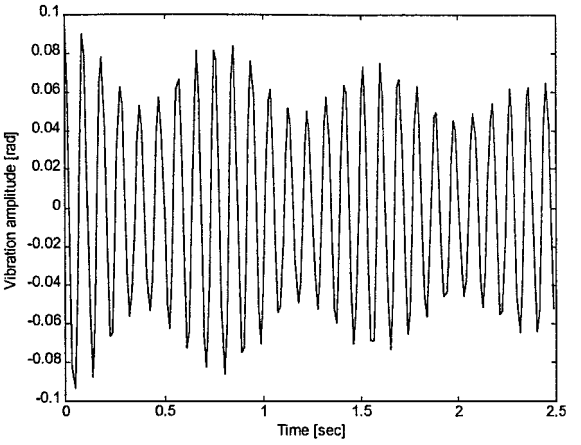

Fig. 10b Blade vibration without blade state feedback; p_1 state is shown.

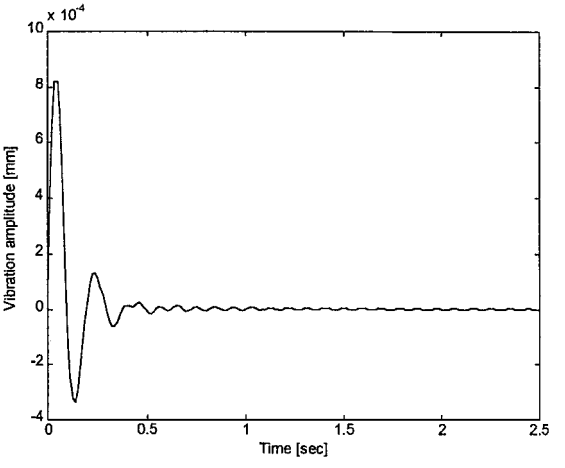

Fig. 11a Hub vibration with blade state feedback; hub axial displacement is shown.

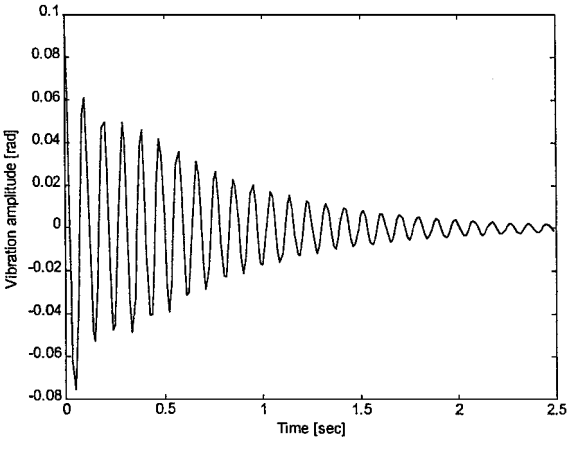

Fig. 11b Blade vibration with blade state feedback; p_1 state is shown.

associated with the blade vibration modes receive almost no damping. The responses show little sign of decay (shown in Fig. 10b). Active control focused on the blade states is needed to suppress the blade vibrations.

An example response of the blade vibration with full state feedback (including the blade states) is shown in Figs. 11a and 11b. The hub vibration levels decrease swiftly (as before) and rapidly die out, shown in Fig. 11a. The blade vibration level (as shown in Fig. 11b) decreases at a steady rate and in a clearly exponentially decaying fashion. This general behavior is true for all of the system vibration modes and strongly illustrates the effectiveness of the proposed strategy to enhance controllability and observability using hub-based actuation and sensing.

Conclusion

The suppression of vibration in multiple rotating airfoil assemblies using hub-based actuators, in the form of magnetic bearings, has been investigated. Modeling issues and associated considerations were described, a simulation model that considered blade flapping was detailed, and control strategies were discussed. Blade mistuning was identified as a strategy to increase hub-based controllability/observability and to allow for greatly improved blade vibration control for multiple airfoil systems. Relative controllability and observability measures were developed and applied to evaluate the proposed mistuning strategy. Simulation results that illustrate the application of this concept were presented and discussed.

Acknowledgments

This work was supported by the National Science Foundation under Grant NSF-CMS-9503488. The government has certain rights in this material. Appreciation is expressed to D. P. Garg for his support of this research effort.

References

[1]Chang, J. C. I., "Integrated Research Approach to Attack Engine HCF Problem," *Proceedings of the ASME Aerospace Division American Society of Mechanical Engineers*, Pub. AD. Vol. 52, American Society of Mechanical Engineers, Fairfield, NJ, 1996, pp. 313–320.

[2]Meher-Homji, C. B., "Blading Vibration and Failures in Gas Turbines Part A: Blading Dynamics and the Operating Environment," *Proceedings of the International Gas Turbine and Aeroengine Congress and Exposition*, 1995; also ASME Paper 95-GT-418.

[3]Gordon, R. W., and Hollkamp, J. J., "Internal Damping Treatment for Gas Turbine Blades," *AIAA/ASME/ASCE/AHS/ASC Structures, Structural Dynamics and Materials Conference*, Vol. 1, AIAA, Reston, VA, 1997. pp. 442–451.

[4]Griffen, J. H., Wu, W.-T., and El-Aini, Y., "Friction Damping of Hollow Airfoils: Part I—Theoretical Development," *Journal of Engineering for Gas Turbines and Power*, Vol. 120, No. 1, 1998, pp. 120–125.

[5]Humphris, R. R., Kelm, R. D., Lewis, D. W., and Allaire, P. E., "Effect of Control Algorithms on Magnetic Journal Properties," *Journal of Engineering for Gas Turbines and Power*, Vol. 108, No. 4, 1986, pp. 624–632.

[6]Williams, R. D., Keith, F. J., and Allaire, P. E., "A Comparison of Analog and Digital Controls for Rotor Dynamic Vibration Reduction Through Active Magnetic Bearings," *Journal of Engineering for Gas Turbines and Power*, Vol. 113, No. 4, 1991, pp. 535–543.

[7]Flowers, G. T., Szász, G., Trent, V. S., and Greene, M. E., "Study of Integrally Augmented State Feedback Control for an Active Magnetic Bearing Supported Rotor System," American Society of Mechanical Engineers, Paper 97-GT-231, 1997.

[8]Carta, F. O., "Aeroelasticity and Unsteady Aerodynamics," *Aircraft Propulsion Systems Technology and Design*, AIAA, Washington, DC, 1989, Chap. 7.

[9]Dowell, E. H., Howard, C. C., Scanlan, R. H., and Sisto, F. A., *Modern Course in Aeroelasticity*, Kluwer Academic, Dordrecht, The Netherlands, 1989, pp. 411–441, Chap. 8.

[10]Szász, G., and Flowers, G. T., "Vibration Control of a Mistuned Bladed Disk Assembly via Magnetic Bearings," *Journal of Vibration and Control*, (to be published).

[11]Pierre, C., and Murthy, D. V., "Aeroelastic Modal Characteristics of Mistuned Blade Assemblies: Mode Localization and Loss of Eigenstructure," *AIAA Journal*, Vol. 30, No. 10, 1992, pp. 2483–2496.

[12]Kielb, R. E., and Kaza, K. R. V., "Effects of Structural Coupling on Mistuned Cascade Flutter and Response," *Journal of Engineering for Gas Turbines and Power*, Vol. 106, No. 1, 1984, pp. 17–24.

[13]Kailath, T., *Linear Systems*, Prentice–Hall, Englewood Cliffs, NJ, 1980, pp. 135–139, 366, Chap. 2.

[14]Hohenemser, K. H., and Yin, S. K., "Some Applications of the Method of Multiblade Coordinates," *Journal of the American Helicopter Society*, Vol. 17, No. 3, 1972, pp. 1–9.